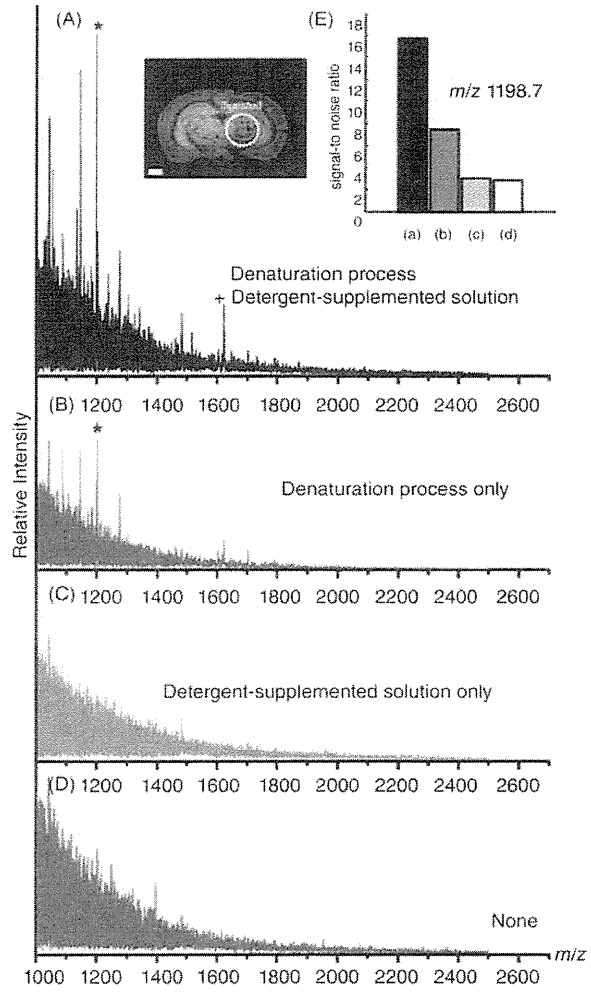

FIGURE 3.9 On-tissue digestion process was enhanced by the heat-denaturation process and the use of detergent-supplemented trypsin solution. A. Mass spectra obtained from 10-μm mouse cerebellum sections of trypsin-digested position (see inset). B–D. Mass spectrum obtained from the tissue sections prepared with indicated treatment of denaturation and detergent. Asterisks represent the mass peaks at *m/z* 1198.7. E. Signal-to-noise ratio of peak at *m/z* 1198.7 obtained from each tissue section. Bar, 1 μm [19].

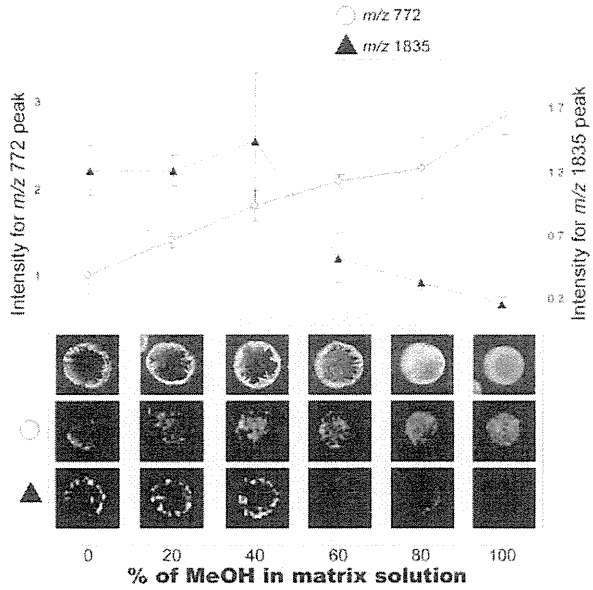

FIGURE 3.10 Concentration of organic solvent in the matrix solution influences signal detection in the analysis of lipids and peptides. The brain homogenate slices were dispensed with 0.1 μL of DHB solutions containing different concentrations of the organic solvent (0%, 20%, 40%, 60%, 80% and 100% methanol containing 0.1% TFA), and the sensitivity of the signals corresponding to endogenous lipids and peptides was measured. The results showed that a high composition of methanol (80%–100%) was favorable for lipid detection, while a low concentration solution (20%–40%) was favorable for the detection of peptides. The crystal form of the analytes also changed with an increase in the methanol concentration in the matrix solution; needle-like crystals from which peptides were detected changed into aggregates of smaller crystals from which lipids were detected.

TABLE 3.2 Potential Contribution of IMS for Imaging of Metabolites in Tissues or Cells

	Representative Molecular Imaging Method in Tissue or Cells	Probes	Selectivity	Allow Simultaneous Imaging
DNA	FISH (fluorescence in situ hybridization)	Oligo nucleotide probe	Targeted	+
RNA	In situ hybridization	Oligo nucleotide probe	Targeted	+
Protein	Immunohistochemistry, green fluorescent protein-fused protein	Antibody	Targeted	+
Metabolite (especially lipids)	Imaging mass spectrometry	–	Targeted/ nontargeted	+++

molecular diversity

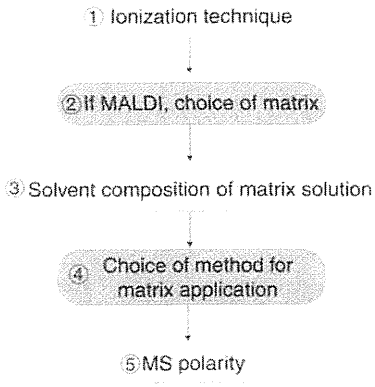

FIGURE 3.11 Representative experimental points to consider in MALDI-IMS of small metabolites.

group in sulfatides. In particular, GPLs is the most frequent studied topic because their rich amounts in the tissues make the analysis easier [30]. However, for analysis of the noncharged and less-abundant molecular components, development of suitable sample preparation protocol to enhance their sensitivity is necessary. This is especially the case for lipid imaging, in which tissue-washing procedure with organic solvents is omitted because lipids are easily lost or migrate from their original location in tissues. When such a crude sample is subjected to MS analysis, numerous molecular species compete for ionization, and this can gives rise to severe ion suppression effects, degrading the sensitivity of such "difficult" lipids [5–7]. Hence, systematical experimental strategies ranging a wide variety of lipid species must be developed for successful lipid IMS. Figure 3.12 shows a proposed experimental strategy for MALDI-IMS of biological lipids. It is reported that proper choice of MS polarity (positive or negative) and use of suitable matrix solution is critical [31,32].

Addition of Salt to the Matrix Solution Enhanced the Sensitivity of Lyso-PC (Polar Lipid) Detection But Decreased the Sensitivity of TG (Nonpolar Lipid) Detection As demonstrated in Figure 3.10, composition of matrix solution is an important and useful "adjustable" parameter to increase the detection sensitivity of target analyte. In addition, if properly used, additive compounds to the matrix solution are another effective factor to achieve selective increase of target analyte signal. In this regard, it is reported that the presence/absence of alkali metal salts in the matrix solution affects the detection sensitivity for polar and nonpolar lipids [32]. Figure 3.13 shows that addition of the potassium acetate to the matrix solution enhanced the sensitivity of lyso-PC (polar lipid) detection, but on the other hand, decreased the sensitivity of triacylglycerol (TG) (nonpolar lipid) detection. The left panel of Figure 3.13 shows that the alkali metal salt in the matrix solution enhanced the sensitivity of phosphatidylcholine (PC) detection, presumably by the merging of $[M+H]^+$ and $[M+K]^+$ ion adduct form into $[M+K]^+$, in the presence of potassium salt additive. Contrastingly, under the presence of a potassium salt, the intensity of TG as the $[M+K]^+$ decreased to approximately half even at 4 mM (right panel). This can be accounted in that the enhancement of ionization for endogenous PCs signals the underexistence of the salt: the signal degradation of neutral lipids was attributed to the ion suppression effect of the enhanced PC ionization.

TABLE 3.3 Summary of Application Studies of MALDI-IMS for Lipids

Complex lipid	**GPLs**
	PCs (Astigarraga et al., 2008 [92]; Garrett et al., 2006 [1]; Jackson et al., 2005a,b [26,54]),
	PEs (Astigarraga et al., 2008 [92]; Jackson et al., 2005a, 2007b [26,58]),
	PIs (Astigarraga et al., 2008 [92]; Jackson et al., 2005a, 2007b [26,58]),
	PSs (Astigarraga et al., 2008 [92]; Jackson et al., 2005a, 2007b [26,58]),
	PGs (Jackson et al., 2005a, 2007b [26,58]), and
	Cardiolipins (Wang et al., 2007 [31])
	Glycosphingolipids
	Gandliosides (Chen et al., 2008 [56]; Sugiura et al., 2008 [93]),
	Sulfatides (Ageta et al., 2008 [94]; Chen et al., 2008 [56]; Jackson et al., 2007b [58]), and
	Galactocyl-ceramide (Cha and Yeung, 2007 [95]; Taira et al., 2008 [23])
Simple lipid	**Neutral lipids**
	Triacylglycerols (Astigarraga et al., 2008 [92]) and diacylglycerols (Astigarraga et al., 2008 [101])
Derived lipid	**Fatty acids** (Zhang et al., 2007 [96])
	Cholesterol (Altelaar et al., 2006 [72]; Jackson et al., 2005a [26])

PC, phosphatidylcholine; PE, phosphatidylethanolamine; PI, phosphatidylinositol; PS, phosphatidylserine; PG, prostaglandin.

Generation of Multiple Molecular Ion Adducts from a Single PC Molecular Species Was Suppressed by Adding an Alkali Metal Salt to the Matrix Solution The addition of alkali metal salts has another advantage: The formation of multiple molecular species with the same nominal mass can be avoided during the analysis of endogenous phospholipids. With the addition of alkali metal salts, the mass spectra of endogenous lipids (in the m/z range of 400–900) are simplified to a

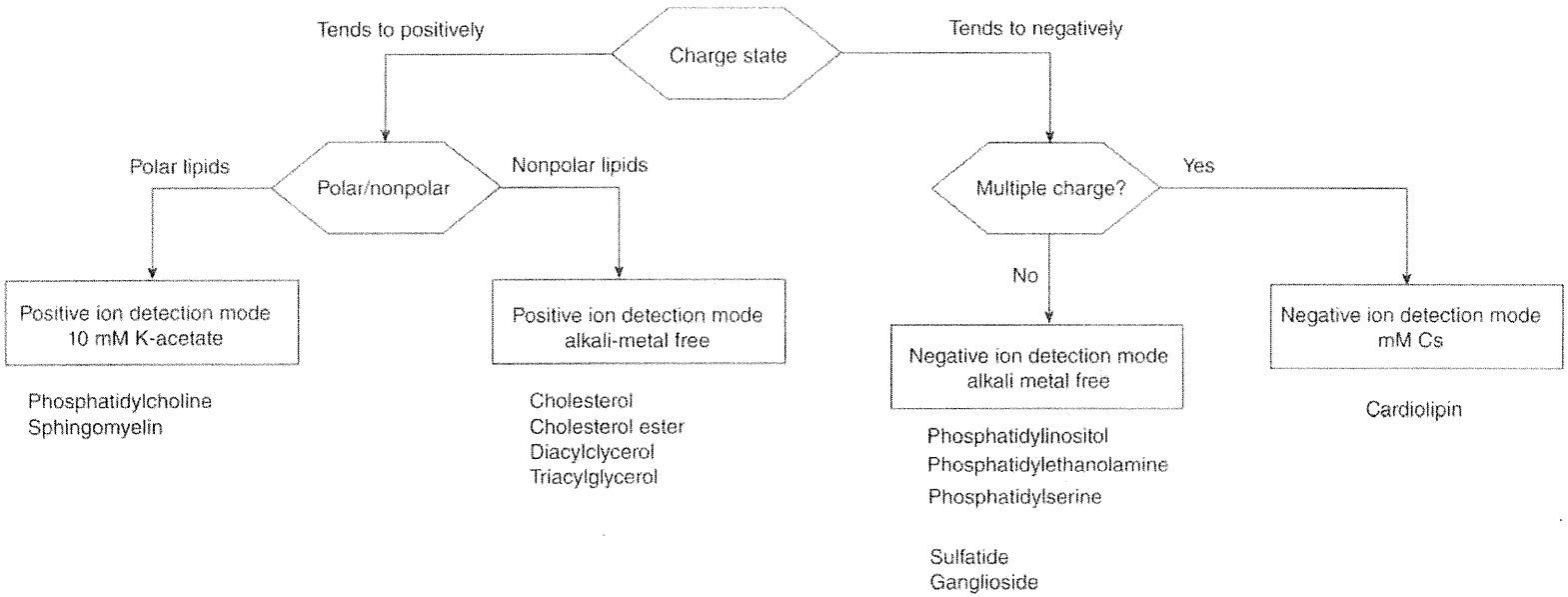

FIGURE 3.12 Suggested experimental procedure for various lipid molecules.

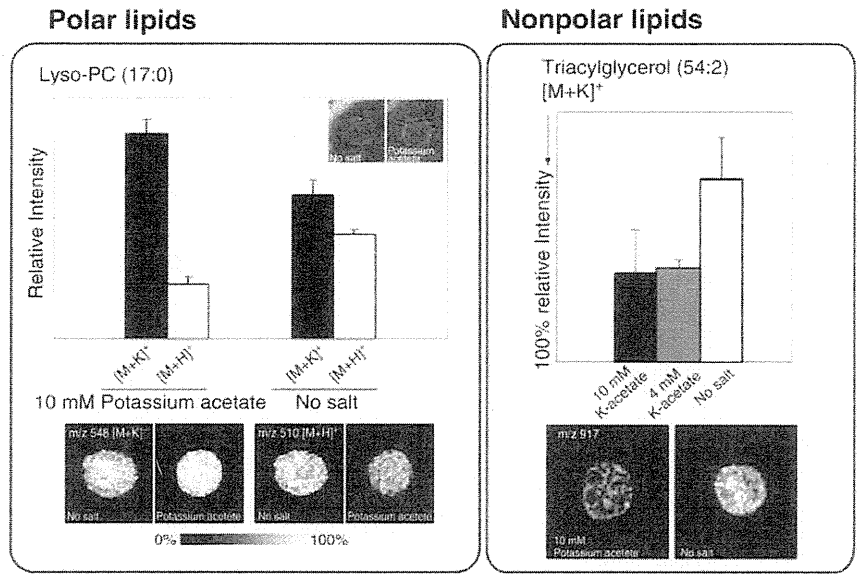

FIGURE 3.13 Addition of the potassium acetate to the matrix solution enhanced the sensitivity of lyso-PC (polar lipid) detection, but on the other hand, decreased the sensitivity of TG (nonpolar lipid) detection. We dispensed the solution of the reference compounds (0.1 μL) on thin sections of the tissue homogenate. We then sprayed the sections with different matrix solutions and measured the sensitivity of detection of each dispensed compound. We tested polar lipids such as lyso-PC and nonpolar lipids such as cholesterol and TG which tend to be charged positively. The results obtained for PC showed that the alkali metal salt in the matrix solution enhanced the sensitivity of PC detection; the most prominent signal derived from lyso-PC(17:0) was attributed to the $[M+K]^+$ ion when using potassium acetate as the additive, while the generation of the $[M+H]^+$ ion was reduced under the condition. These results can be accounted for the merging of ion adduct form into $[M+K]^+$ in the presence of potassium salt additive. On the other hand, alkali metals salts added to the matrix solution during the detection of nonpolar lipids caused a decrease in the signal sensitivity.

considerable extent since multiple adduct ions formed are merged into a single alkali adduct ion. Figure 3.14 shows the representative mass spectra obtained from the rat kidney sections both in the presence/absence of 10 mM potassium acetate. Since PCs preferentially form cations in the form of alkali metal adducts [26,33,34] and tissues are rich in sodium and potassium salts, peaks due to $[M+H]^+$, $[M+Na]^+$, and $[M+K]^+$ ions are detected in the mass spectra of endogenous PCs (Figure 3.14A). This is a critical problem that needs to be addressed because many molecular species are generated from PCs, and hence, a single peak in the spectrum may correspond to multiple ions. Table 3.4 summarizes the *m/z* values of abundant brain PCs in various ion forms, and it demonstrates that many molecular species share the same nominal mass (as indicated by the same fonts or styles). For example, the mass of a protonated PC(diacyl-16:0/20:4) molecule is identical to that of a sodiated PC(diacyl-16:0/18:1) ion (*m/z* 782), as can be seen in Figure 3.14A. In fact, MS/MS analysis of the peak appearing at *m/z* 782 in the absence of the potassium salt shows that this peak actually corresponds to three different PC ions: $[PC(diacyl\text{-}16:0/20:4)+H]^+$, $[PC(diacyl\text{-}16:0/18:1)+Na]^+$, and $[PC(1\text{-}alkyl\text{-}16:0/18:2)+K]^+$. This can be confirmed from the MS/MS spectra shown in Figure 3.14B(e–f); the peak at *m/z* 782 corresponds to three type of PCs which are a protonated PC ion (by a diagnostic peak at *m/z* 184 [a]), a sodiated PC ion (by *m/z* 147 [b]), and a potassiated PC ion (by *m/z* 163 [c]). On the other hand, upon addition of the potassium salt, peaks due to the aforementioned forms of the PC ions were separated into two distinct peaks at *m/z* 798 and 820, corresponding to $[PC(diacyl\text{-}16:0/18:1)+K]^+$ and $[PC(diacyl\text{-}16:0/20:4)+K]^+$, respectively (Figure 3.14A). In addition, MS/MS analysis of the spectra clearly shows that only potassiated PC molecules are present in the mass peaks (Figure 3.14B[g–h]). As can be seen from Table 3.4, by merging into $[M+K]^+$ ion, most of such mass sharing of abundant PC species can be avoided except that of isobaric species.

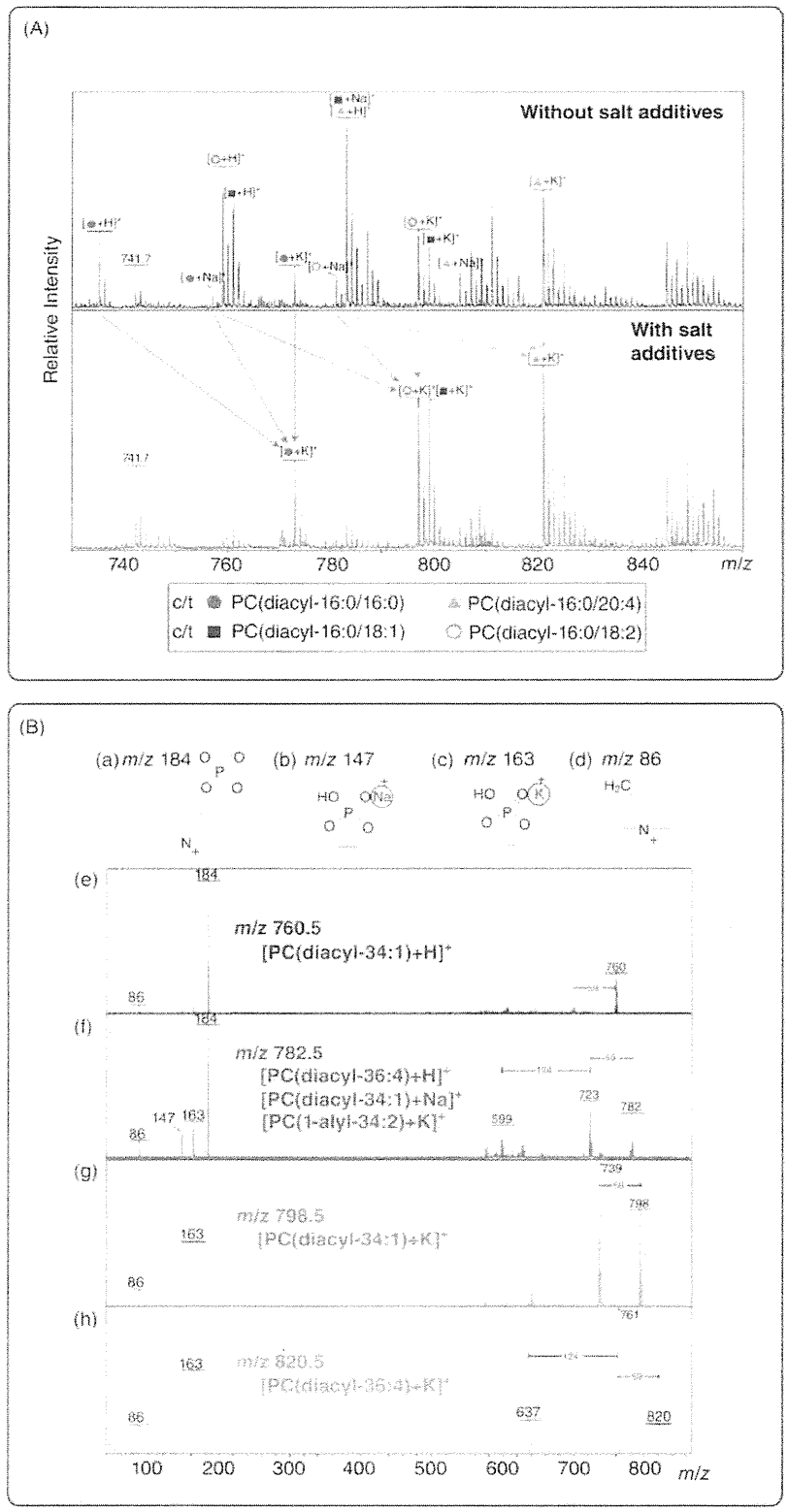

FIGURE 3.14 Generation of multiple molecular ion adducts from a single PC molecular species was suppressed by adding an alkali metal salt to the matrix solution. A. Generation of multiple molecular ions from a single PC molecule was suppressed by adding an alkali metal salt to the matrix solution. Spectra obtained from sections of rat brain homogenate in the presence/absence of potassium acetate in the matrix solution are shown. With the addition of potassium acetate to the matrix solution, multiple molecular ion forms of PCs merged into a single potassiated PC ion. B. Structure of the diagnostic ions for (a) protonated PC at *m/z* 184; (b) sodiated PC at *m/z* 147; (c) potassiated PC at *m/z* 163. MS/MS spectra of ion peaks at (e) *m/z* 760 and (f) 782 in the absence of potassium acetate and spectra of ions peaks at (g) *m/z* 798 and (h) 820 in the presence of potassium acetate are also shown. c/t, corresponding to.

TABLE 3.4 The *m/z* Values of Abundant Brain PCs as Various Ion Forms

Molecular Species	PC	$[M+H]^+$	$[M+Na]^+$	$[M+K]^+$
PC(diacyl 16:0–18:1)	C34:1	760	782	798
PC(diacyl 16:0–16:0)	C32:0	734	756	772
PC(diacyl 18:0–18:1)	C36:1	788	*810*	826
PC(diacyl 16:0–20:4)	C36:4	782	804	820
PC(diacyl 16:0–18:0)	C34:0	762	784	800
PC(diacyl 16:0–22:6)	C38:6	**806**	828	844
PC(diacyl 18:0–20:4)	C38:4	*810*	***832***	848
PC(diacyl 18:1–20:4)	C38:5	**808**	830	846
PC(diacyl 18:0–22:6)	C40:6	834	856	872
PC(diacyl 18:1–18:1)	C36:2	786	**808**	824
PC(diacyl 16:0–16:1)	C32:1	732	754	770
PC(diacyl 18:1–22:6)	C40:7	***832***	854	870
PC(diacyl 16:0–20:3)	C36:3	***784***	**806**	822
PC(diacyl 18:0–18:2)	C36:2	786	**808**	824
PC(diacyl 18:1–18:2)	C36:3	***784***	**806**	822

For Negatively Charged Lipids Containing Multiple Negative Charted Structures, Addition of Alkali Metal Salt Enhanced Generation of Singly Charged Molecular Ions Alkali-metal salts dissolved in the matrix solution enhanced generation of singly charged ion molecules which contain the multiple negatively charged structures; during ionization, residual charged groups in their structures were neutralized by adduct formation with alkali metal cations, and as a result, singly charged ions could be efficiently generated. Since in MALDI process, much less multiple charged ions could be generated than that of ESI, the salt addition eventually can improve their sensitivity by promoting the efficiency of single-charged ion generation.

In the study of Hay-Yan J. Wang et al., they added 100 mM of cesium iodide to a matrix solution (docosahexaenoic acid [DHA] 30 mg/mL in 50% ethanol) and successfully profiled multiple species of cardiolipin as single-charged molecular ions by neutralizing additional phosphate group (Figure 3.15). This treatment also benefits to integrate the ion adduct form to $[M+Cs-2H]^-$ [31]. That may be the case for gangliosides, which have multiple sialic acids in their sugar chain. Taken together, for the analysis of lipids which tend to have multiple charges, the addition of appropriate concentration of alkali metal salt is advantageous (Figure 3.12).

MALDI-IMS of Phospholipids Revealed Cell-Selective Production of PC Molecular Species GPLs comprise a large molecular family in which phosphoric acid is esterified to a glycerolipid. They are subdivided into distinct classes (e.g., PCs, phosphatidylethanolamines, and phosphatidylinositols) based on the structure of the head group linked to the phosphate, attached at the *sn-3* position of the glycerol backbone. They are further subdivided into numerous molecular species on the basis of the composition of the fatty acids linked to the *sn-1* and *sn-2* positions of the glycerol backbone [30]. Using IMS, we can image not only these multiple classes but also related molecular species simultaneously. In particular, the capability to determine the distinct localization of each molecular species, that is, to elucidate the distinct fatty acid composition of biological membranes in different tissue locations, is an important advantage of IMS [30] (Figure 3.16).

In the brain, among the classes of GPLs, PCs are the most abundant structural component of neural and glial cell membranes, and the fatty acid constituents of PCs (i.e., molecular species) influence the membrane's physical properties, including fluidity and curvature [35–38]. Since several types of fatty acids, especially polyunsaturated fatty acids (PUFA), in the PCs are released and converted in response to extracellular stimuli into bioactive lipids that mediate important biological processes [39], information on the distinct distributions of PUFA-containing molecular species is quite valuable [40,41]. By applying high-magnification IMS to the cerebella cortex, a docosahexaenoic acid-containing phosphatidylcholine (DHA-PC), namely PC(diacyl-18:0/22:6), was found to be enriched in the Purkinje cell layer (Figure 3.17). Optical observation of successive hematoxylin and eosin (HE)-stained brain sections also suggested that PC(diacyl-18:0/22:6) was selectively detected in Purkinje cells (Figure 3.17, arrowheads) and in molecular layers (MLs) in which dendrites of Purkinje cells exist. In contrast, granule cells were impoverished in another DHA-PC, namely PC(diacyl-18:0/22:6). Interestingly, a complementary distribution of two other

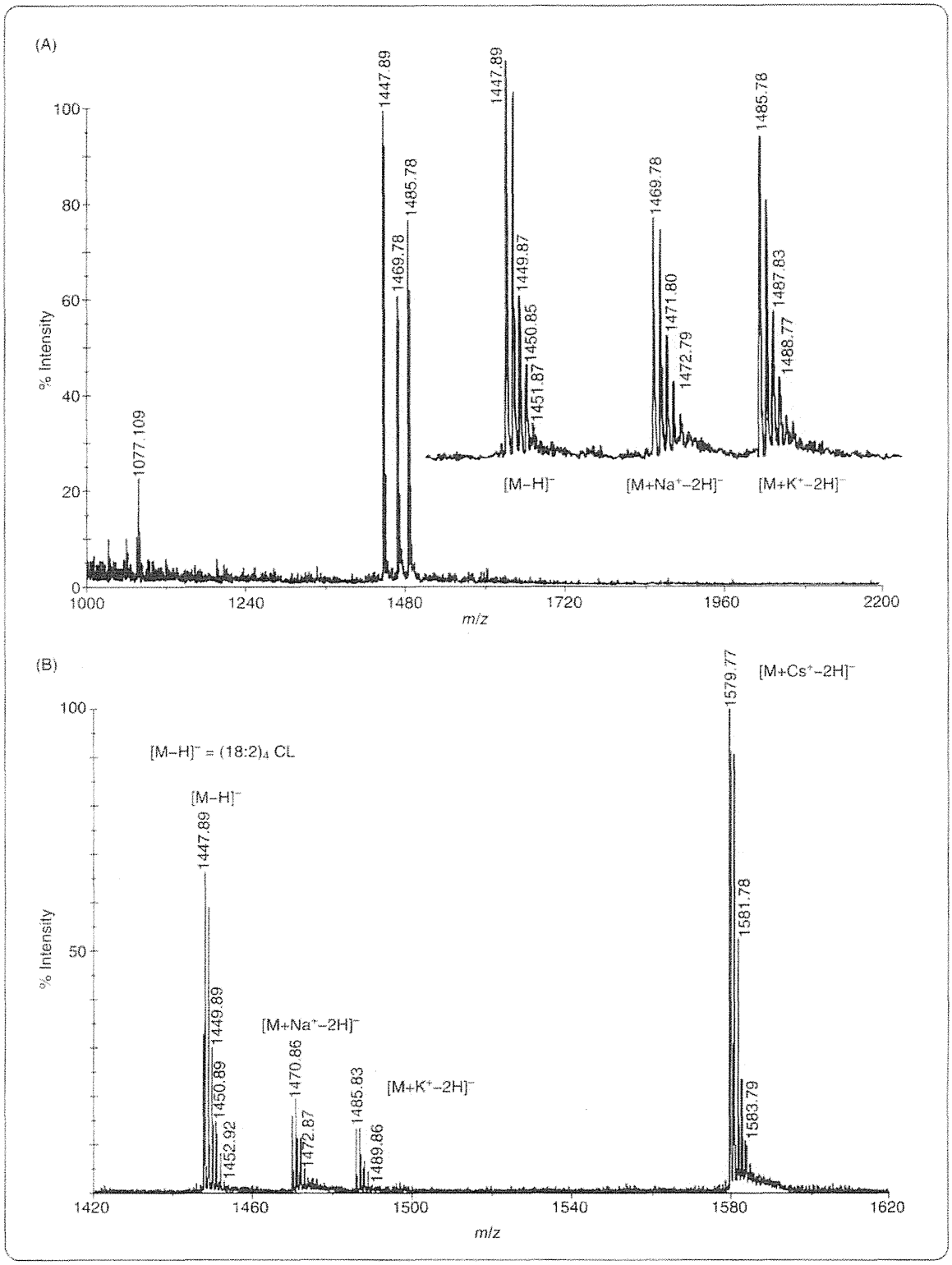

FIGURE 3.15 Detection of cardiolipins as cesium (Cs)-adducted negative ions. A. MALDI-MS spectrum of $(18:2)_4$ cardiolipin (CL) from rat heart section. The inset magnifies the *m/z* region between 1420 and 1520. DHA matrix was used at 30 mg/mL. B. MALDI-MS spectrum of $(18:2)_4$ CL from rat heart section in the presence of Cs ions. The relative abundance of sodiated and potassiated CL was significantly decreased by Cs addition [31].

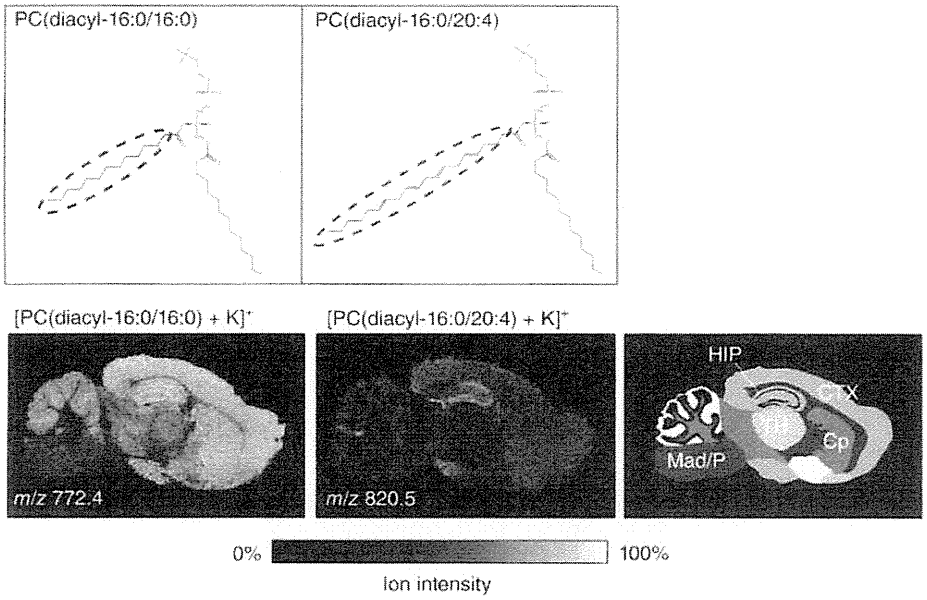

FIGURE 3.16 Distinct localization of phospholipid molecular species revealed by IMS. Different distribution pattern of phospholipids arise from the distinct fatty acid composition of GPLs.

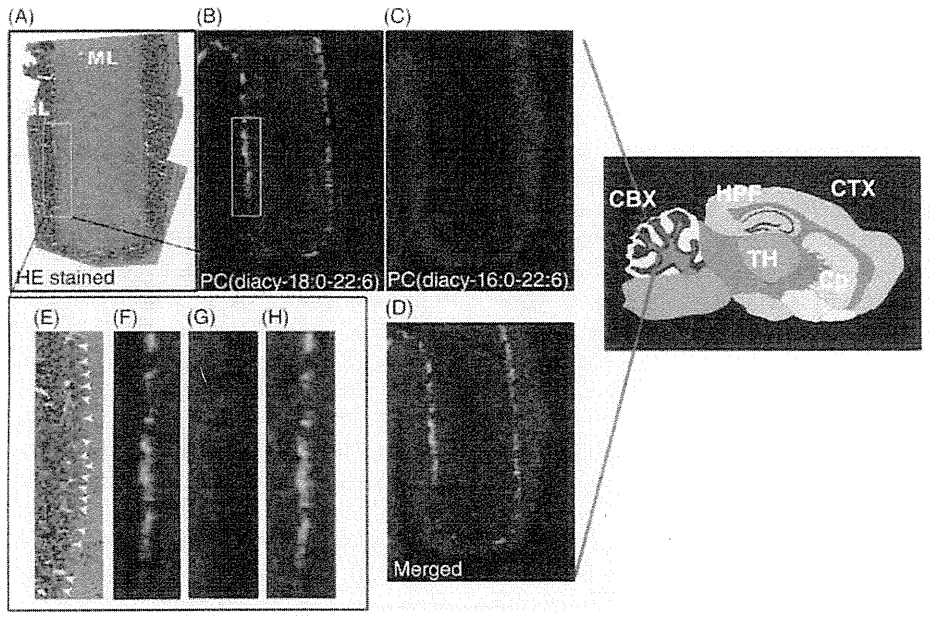

FIGURE 3.17 Purkinje cells selectively contained a DHA-PC. High-magnification IMS at raster size of 15 μm revealed the Purkinje cell-selective distribution of PC(diacyl-18:0/22:6) in the cerebellum. Both optical observation of HE-stained successive brain sections (A, E) and ion images of DHA-PCs (B, F) clearly suggest that the PC was enriched in the Purkinje cell layer (arrowheads). Interestingly, a complementary distribution of another abundant DHA-PC, PC(diacyl-16:0/22:6), was enriched in the granule layer of the cerebellum (C, G). D. Merged image. ML, molecular layer; GL, granule layer; W, white matter; CBX, cerebellar cortex; CP, corpus striatum; CTX, cerebral cortex; HPF, hippocampal formation; TH, thalamus [41].

abundant DHA-PCs, PC(diacyl-16:0/22:6) and PC(diacyl-18:1/22:6), was observed in the granule cells of the cerebellum (Figure 3.17c,d). Such cell-type heterogeneity of the fatty-acid constituent in part reflects the cells' heterogeneous membrane properties. Because of its high degree of unsaturation, DHA-GPLs increase membrane fluidity and even regulate the functions of membrane-associated proteins [42–44]. Purkinje cells are the largest neurons in the brain, with intricately elaborate dendritic arbors. Thus, higher membrane fluidity may be required for effective transport of membrane-associated proteins via the plasma membrane. Thus, the high-level expression of a DHA-PC may contribute to the transportation of membrane proteins in the cells.

3.2.2.3 *IMS of Endogenous Metabolites: Gangliosides*

Gangliosides are glycosphingolipids consisting of mono- to polysialylated oligosaccharide chains of variable lengths attached to a ceramide unit. They are inserted in the outer layer of the plasma membrane, with the hydrophobic ceramide moiety acting as an anchor while their oligosaccharide moiety is exposed to the external medium [45]. Gangliosides also comprise a large family; their constituent oligosaccharides differ in glycosidic linkage position, sugar configuration, and the contents of neutral sugars and sialic acid. Along with the oligosaccharide unit, the ceramide moiety of gangliosides also varies with respect to the type of long-chain base (LCB) (sphingosine base) and the fatty acid to which it is coupled (Figure 3.18).

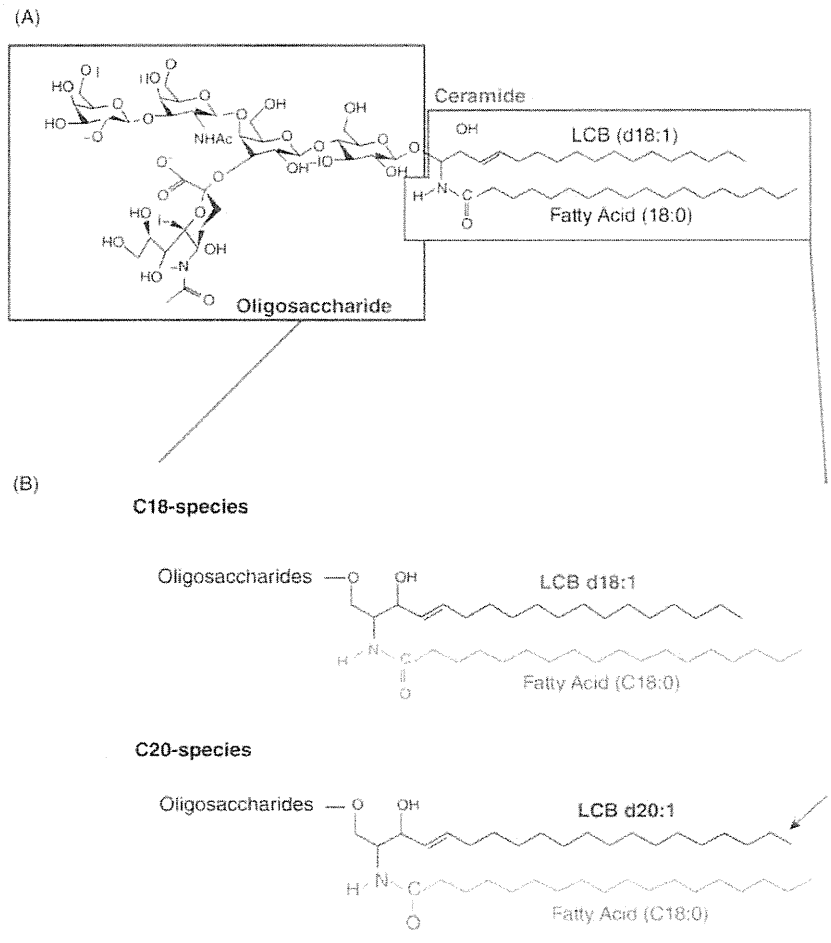

FIGURE 3.18 Structure of GM1a. Gangliosides comprise a large family; their oligosaccharides structures differ in the glycosidic linkage position, sugar configuration, and the contents of neutral sugars and sialic acid content. The ceramide moiety of gangliosides also has some variation with respect to the type of long-chain base (LCB) (sphingosine-base) and fatty acid moiety (A). Structures of ganglioside molecular species containing C18- and C20-long chain base (LCB) are shown in (B).

Previous biochemical studies have revealed that the LCB of the brain ganglioside species has either 18 or 20 carbon atoms (i.e., C18- or C20-sphingosine), and C20-sphingosine (C20-LCB species) is present in significant amounts only in the central nervous system [46–49]. The LCB content increases significantly in rodents and humans throughout life [50–52]. The C20-LCB gangliosides are of great interest because of their characteristic brain specificity and their dramatic increase during the organism's life span. However, the field lacks the capability to provide a precise tissue distribution of C18 and C20 gangliosides. Antibodies to some oligosaccharide moieties are available for visualizing the molecular species with different constituent oligosaccharides [53], but such immunological methods cannot detect the differences in the ceramide structure hidden in the lipid bilayer.

Due to the negative charge on the sialic acids and their rich abundance in the brain, gangliosides are easily detected in the *m/z* 1500–2500 range with IMS in the negative ion detection mode [54–56]. In addition, IMS discriminates not only structural differences in oligosaccharides but also in the lipid moiety, and therefore, the specific distribution of the C20-LCB species is successfully revealed in the mouse brain. While the C18 species is widely distributed throughout the frontal brain, the C20 species is selectively localized in the ML of the dentate gyrus (DG) (Figure 3.19). Furthermore, the developmental- and aging-related accumulation of the C20 species in the ML-DG can be visualized [55], therefore the tissue location of C20 gangliosides accumulation can be identified (Figure 3.20).

These observations indicate that this brain region-specific regulation of LCB chain length is, in particular, important for its distinct function in the brain. As this study clearly demonstrates, the novel capabilities of IMS could shed light on long-standing questions in the biological/clinical field.

3.2.2.4 IMS of Endogenous Metabolites: Primary Metabolites In the body, primary metabolites are directly involved in normal growth, development, and reproduction processes. Most of these molecules are smaller than typical lipids (<*m/z* 600) and regarding the imaging of such low molecular weight compounds, one of the disadvantages of organic matrices is the number of observed mass peaks in the low *m/z* range. The low *m/z* region of a MALDI spectrum contains a large population of ions from endogenous metabolites as well as matrix-related adduct clusters and fragments which are clearly seen in the MALDI ion mobility spectrum obtained on the tissue section [1,57]. Such high density of ions increases the risk for sharing the same mass window by matrix ions and analyte molecules [58] (Figure 3.21). One of the effective solutions to avoid this problem is search and development of the new matrix compounds suitable to the direct-tissue MS.

Recently, 9-aminoacridine (9-AA) was found to exhibit very few matrix interferences in the low-mass range (*m/z* < 500) [59] and thus primary metabolites can be visualized in a MALDI imaging experiment [60,61]. Benabdellah et al. reported that with appropriate sample preparation protocol, 9-AA exhibits almost no matrix interference, and they successfully detected and identified 13 primary metabolites (adenosine monophosphate [AMP], adenosine diphosphate [ADP], adenosine triphosphate[ATP], uridine diphosphate-N-acetylglucosamine [UDP-GlcNAc], etc.) on the rat brain section in the negative ion detection mode [61]. In another report, Burrell et al. also demonstrated that, by use of the 9-AA in positive ion detection mode, localization of sugar and phosphorylated metabolites such as glucose-6-phosphate can be clearly imaged in plant seeds [60].

Here again, we would like to emphasize that the optimization process of the matrix solution is the critical issue; Figure 3.22 demonstrates that only with appropriate solution composition could the adenosine nucleotides be detected significantly. Before imaging experiment, we have to test several solution compositions with consideration of the solubility, pH stability and heat stability of the target analytes, but since the analyte is cocrystallized with numerous other biomolecules on the tissue surface, in practical, the optimal condition is different from that of purified sample of the same molecule. Actually, as shown in Figure 3.22, we found that 70% ethanol solution is the best for the nucleotides though they have low solubility to such organic solvents. In addition, we also observed that trifluoroacetic acid (TFA) in the solution severely prohibited the ionization of the nucleotides. We eventually determined the optimized condition as 9-AA (10 mg/mL) in the 70% ethanol. Adenosine nucleotides, especially ATP, is well known as the "molecular unit of currency" of intracellular energy transfer [62]. Cellular metabolic processes that use ATP as an energy source convert it into ADP and AMP; therefore, simultaneous imaging of these molecules by IMS provides valuable information regarding tissue metabolic activity. As shown in Figure 3.23, we could simultaneously visualize the distribution pattern of ions for AMP, ADP, and ATP, and furthermore, MS/MS analysis successfully validates these molecular assignments. Finally, we additionally note that because of the in-source decay, the phosphate groups of ATP and ADP may be dissociated and they could be detected as ADP and AMP. In this context, further studies to suppress the in-source fragmentation of phosphate groups are the next issue to consider.

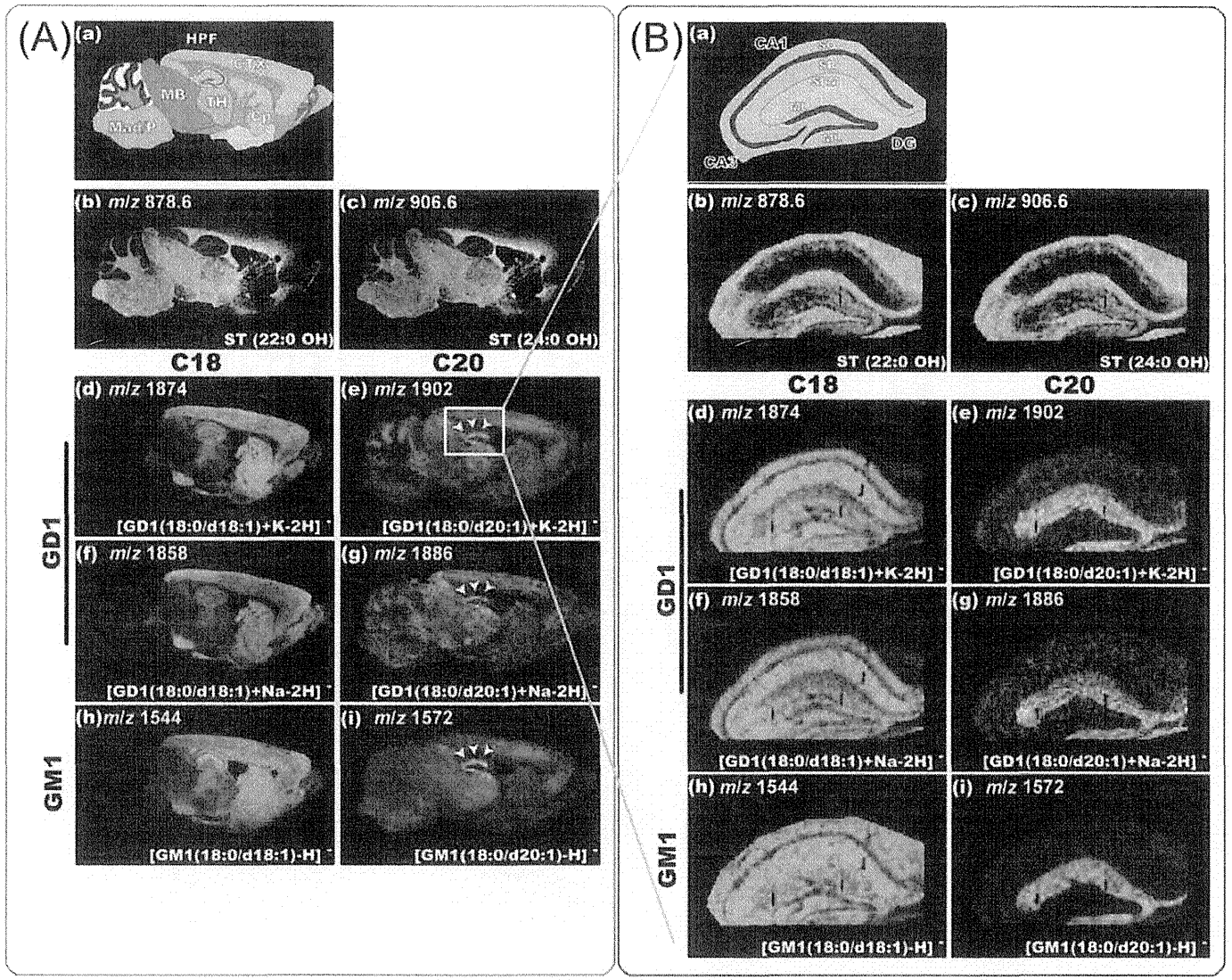

FIGURE 3.19 Localization of C20-sphingosine-containing gangliosides in the hippocampal formation. A. IMS at 50 µm raster step size was used to gain an overview of ganglioside distribution in different brain regions. B. IMS at 15 µm raster size was used to study in detail the distribution pattern of gangliosides in the hippocampus. In both panels, the schematic diagram of the brain section (a) and ion images of STs (b and c) are presented. For ions corresponding to the GD1 molecular species, the ion distributions of both sodium and potassium complexes, that is, the ions at *m/z* 1858 (f) and *m/z* 1886 (g), which correspond to the $[M+Na-H]^-$ form of C18- and C20-GD1, and those at *m/z* 1874 (h) and *m/z* 1902 (i), which correspond to the $[M+K-H]^-$ form of C18- and C20-GD1, respectively, were observed. The ion distribution patterns corresponding to the GD1-Na salts and GD1-K salts are fairly uniform for both C18- and C20-species. For GM1, *m/z* 1544 (d) and *m/z* 1572 (e), which correspond to C18- and C20-sphingosines containing GM1, respectively, are shown.

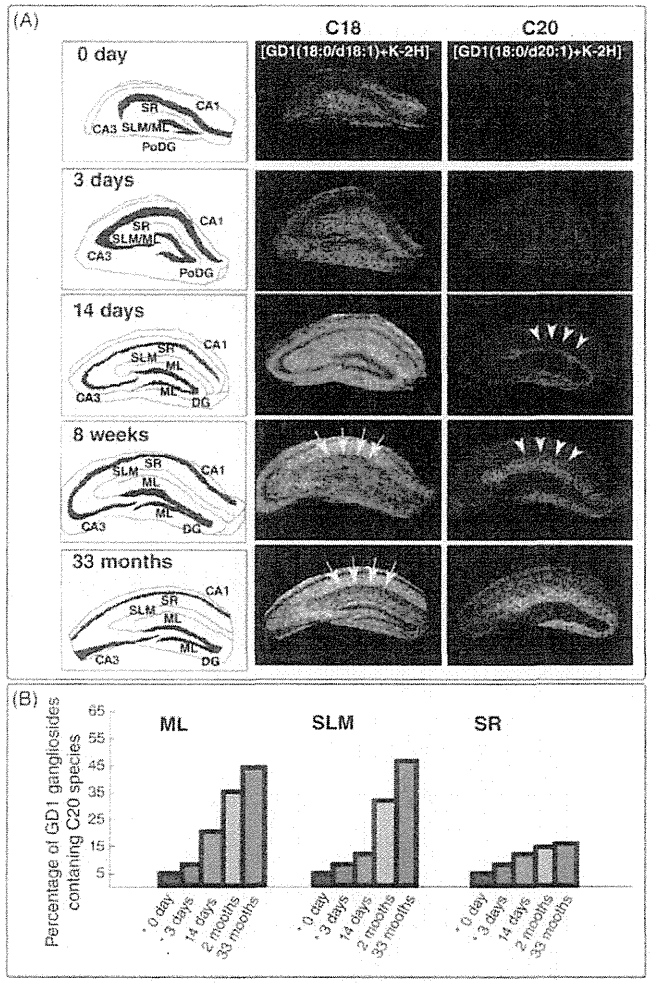

FIGURE 3.20 Development- and aging-related accumulation of C20-GD1 in the ML and stratum lacunosum moleculare (SLM) of the hippocampal formation. It was visualized that the ion corresponded to GD1 (*m/z* 1874 and 1902) in the mouse hippocampus at the indicated time points (P0, P3, P14, 1 month, and 33 months). For each time point, the intensity scale of C20-GD1 is normalized in order that the brightest pixels of C20-GD1 have 60% of the maximal C18-GD1 intensity value. In the P14 mouse hippocampus, C20-GD1 was concentrated in the narrow area of dentate gyrus–middle layer of stratum moleculare (DG-SMm) and began to spread over the medial edge of the region (arrowheads). In contrast, the concentration of the C-18 species decreased in the ML/SLM with aging (arrows). Quantification result of C20-GD1 on the total GD1 signal in the ML, SLM, and stratum radiatum (SR) regions has also been shown (B). *At P0 and P3, we could not distinguish between the ML and SLM areas; therefore, values obtained from the region corresponding to ML/SLM have been used for both regions in the graph.

3.2.3 IMS of Exogenous Drugs

In drug discovery and development, it is a crucial process to determine how a candidate compound is distributed and metabolized within the body. The use of IMS to monitor drug delivery and their metabolism has also been attractive application area. IMS offers detailed drug distribution images, which are comparable to traditional whole body autoradiography (WBA) technique using radiolabeled compounds (Figure 3.24). Stoeckli et al. show these two methods produce remarkably similar results, by performing the IMS and WBA using whole-body sections of the same rat after intratracheal administration of a compound (0.5 mg/kg); intense signals are detected in the trachea, the lung, and the stomach while low levels are detected in the blood, and this reports have nicely introduced the usefulness of IMS for pharmacology.

In addition to that, IMS provides several advantages for determining drug distribution. First, MS-based

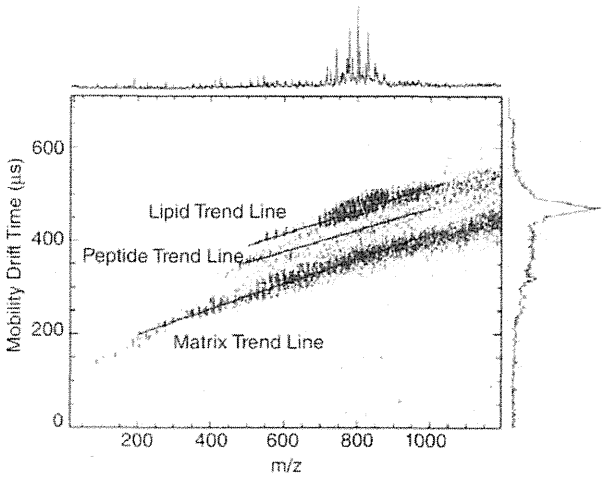

FIGURE 3.21 MALDI-ion mobility 2D plot of a rat brain tissue section with DHB matrix in positive ion detection mode. Many of the peaks in the trend line identified as "matrix" can be assigned to DHB clusters or DHB clusters + potassium. Reprinted from Jackson et al. [58].

molecular detection enables simultaneous and discriminative monitoring of both the intact drug molecules and their metabolites [2,57]. By its nature, WBA cannot distinguish these molecules. In this regard, IMS can determine whether medicinally intact drugs have reached the target organs. Moreover, IMS can provide a visual distribution of drugs at a lower cost and in a much shorter time than detection using isotopes [63]. Khatib-Shahidi et al. have successfully investigated the distribution of olanzapine and its metabolites in a whole rat sagittal section 2 and 6 h after administering the dose [2]. This study clearly showed the distinct distribution of intact drugs and their metabolites; the intact drug reached the target organ (the brain), whereas its metabolites were localized in the bladder. Furthermore, the time course of the metabolism of parent drugs into demethylated and hydroxymethylated metabolites were visualized over the whole-body section. In this study, notable decreases of olanzapine were observed everywhere in the body except the testis and bladder, while the metabolized compounds accumulated in the bladder [2] (Figure 3.25). This example demonstrates that IMS-based drug monitoring provides valuable information for drug development.

On the other hand, ion suppression effects should be considered. In fact, Stoeckli and colleagues have shown that there are small regions (although less than 5% of the total region) where the drugs could not be detected, presumably because of ion suppression effects using a mouse whole-body section coated with analyte drugs

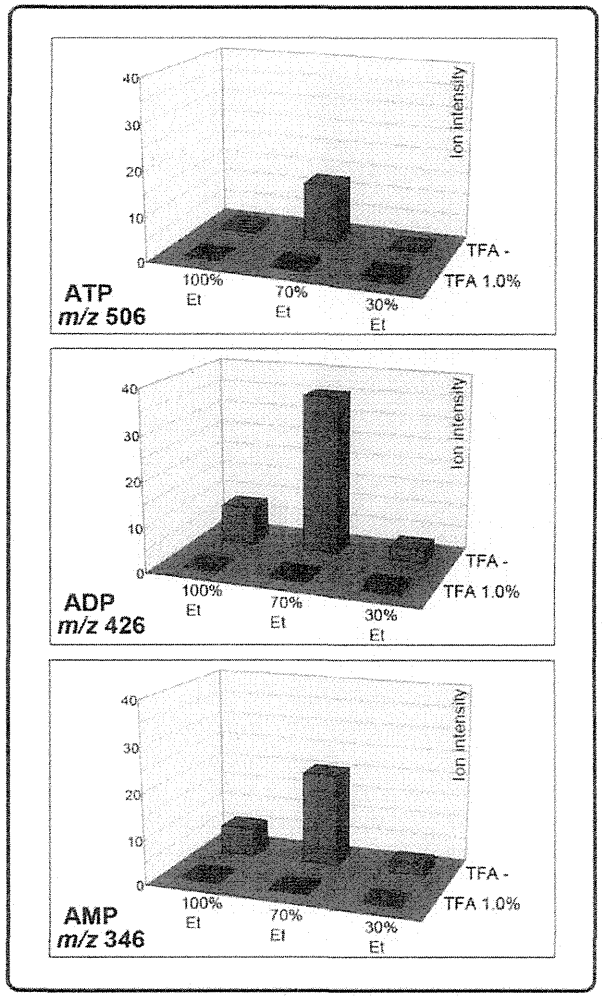

FIGURE 3.22 Optimization of solvent composition for IMS of nucleotides. On the tissue section of mouse heart, AMP, ADP, and ATP were profiled by MALDI-IMS with 9-AA (10 mg/mL) dissolved into different solvent composition of matrix solution. One microliter (1 μL) of each matrix solution were spotted on the sections, and these matrix spots were raster scanned. Indicated ion intensities for AMP (at *m/z* 346), ADP (at *m/z* 426), and ATP (at *m/z* 506) were obtained from averaged mass spectra of each spots. Et, ethanol.

[63]. Thus, optimization of the sample condition so that the analyte molecule present in the crude mixture can be efficiently ionized is an important issue. For this purpose, sample preparation has a critical role. In particular, it is helpful to perform a preliminary experiment using a reference drug because the choice of a suitable matrix compound, as well as optimizing the composition of the matrix solution, can improve the ionization efficiency of the molecules of interest.

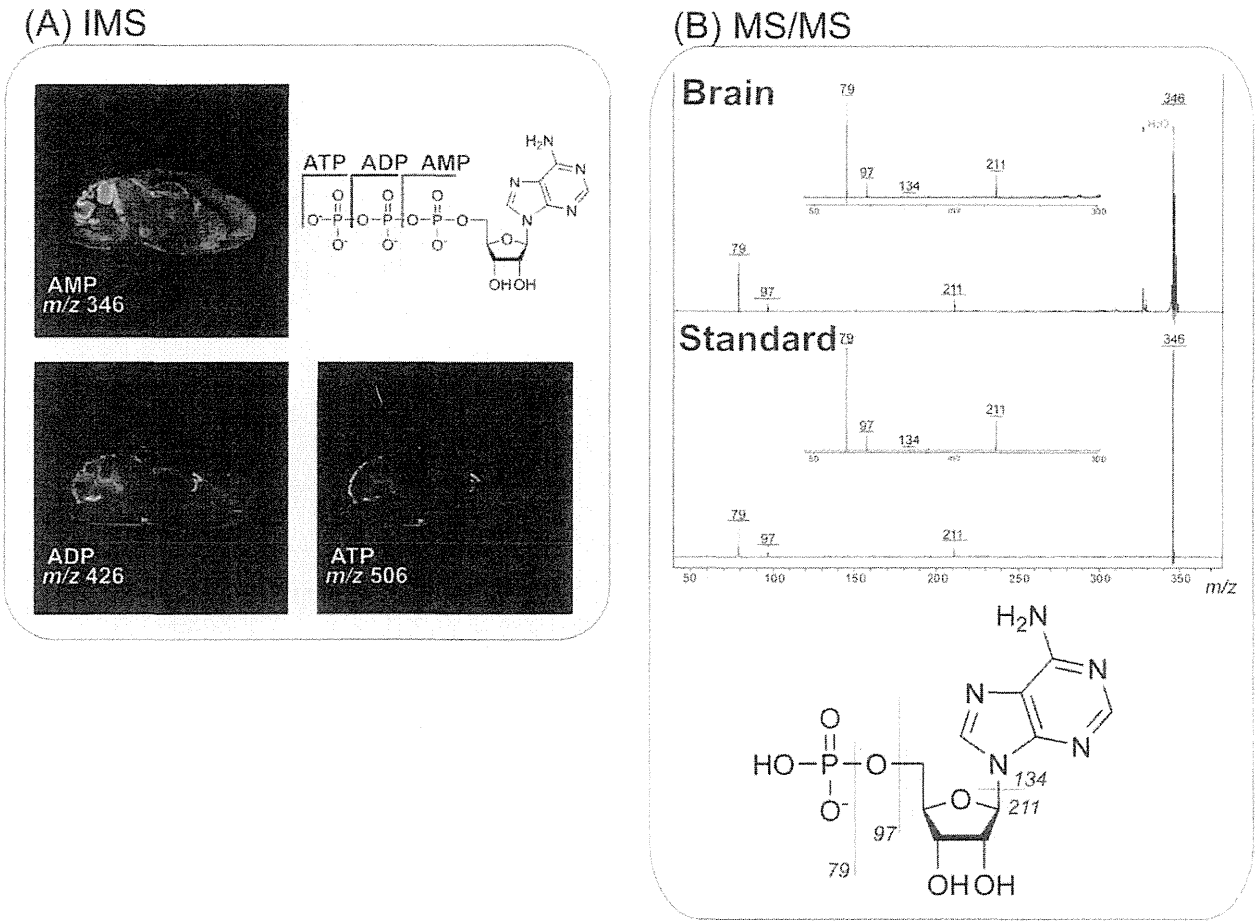

FIGURE 3.23 MALDI-IMS application to adenosine nucleotides. A. Imaging results for AMP, ADP, and ATP with use of 9-AA matrix solution (10 mg/mL in 70% ethanol) at raster scan pitch of 80 μm. B. MS/MS results of the precursor ion at *m/z* 426 acquired from standard sample and brain tissue section. Observed fragmentation pattern indicates that the precursor ion was derived from $[AMP\text{-}H]^-$. The data were obtained with TOF/TOF instrument (Ultra FlexIII, TOF/TOF, Bruker Daltonics).

3.3 EXPERIMENTAL PROCEDURES

In this section, we will introduce the principle and overview of MALDI-IMS and its representative applications. In the following part, the detailed IMS experimental procedures and practical point-to-point techniques will be described; especially for the major IMS application that involves protocol for PC and gangliosides, their results are shown in Figures 3.16, 3.17, 3.19 and 3.20, respectively.

3.3.1 Materials

3.3.1.1 Chemicals

1. TFA
2. 1,2-dihexanoyl-*sn*-glycero-3-phosphocholine (MW: 453.5, monomer and dimmer were used for calibration) and peptide calibration standard II (Bruker Daltonics, Leipzig, Germany; covered mass range: ~700–3200 Da) as a calibration standard
3. DHB (Bruker Daltonics) as a matrix

Note: All of the chemicals used in this study were of the highest purity available.

3.3.1.2 Matrix Solution for MALDI-IMS of PCs For measurement of PC, a DHB solution (40 mg/mL DHB, 10 mM potassium acetate, 70% methanol, 0.1% TFA) was used as the matrix solution [41].

3.3.1.3 Matrix Solution for MALDI-IMS of Gangliosides For measurement of gangliosides, a matrix solution without salt (40 mg/mL DHB, 70% methanol, 0.1% TFA) was used as the matrix solution [55].

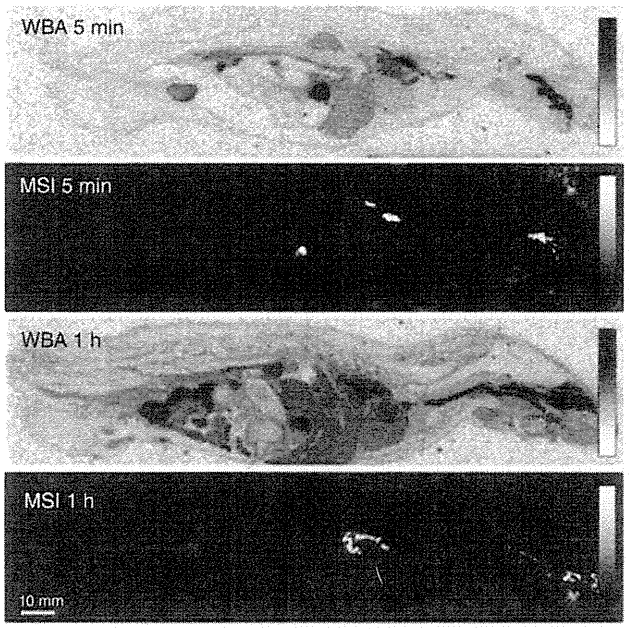

FIGURE 3.24 Comparison of IMS with WBA using whole-body sections after intratracheal administration of a compound (0.5 mg/kg) to rats. The two corresponding sections are from the same animal, but from different positions. Comparison of the methods shows remarkable similarity in the results: high levels are detected in the trachea, the lung, and the stomach, and lower levels in blood. MSI (mass spectrometry imaging) is used as a synonym of IMS [63].

Note: The potassium, sodium, and lithium alkali metals show a distinct ability to form adducts with the PC molecule. We recommend adding 10 mM potassium salt because potassium forms a stronger adduct with PC molecules than did other metals. Figure 3.26 shows that potassium ions formed stronger adducts with the PC molecules than did sodium and lithium ions. Addition of 10 mM of potassium acetate to the matrix solution resulted in the dominant formation of the $[M+K]^+$ ion. On the contrary, other types of PC ions still accounted for approximately 50% on total intensity after the addition of 20 mM sodium and lithium acetate.

3.3.2 Methods

3.3.2.1 Animal Sacrifice and Tissue Extraction All experiments involving mice were conducted in accordance with the protocols approved by the animal care and use committee at the participating research institute.

1. The brains of 8-week-old male C57BL/6J Cr mice were used.
2. The brains were extracted within 1 min (typically 40 s) after sacrifice (see note below).
3. The trimmed tissue blocks were immediately frozen in powdered dry ice, which allows tissues to be frozen without cracks, and stored at –80°C until use.

   Note: As shown in Figure 3.27, postmortem degradation of GPLs was observed by IMS within 15 min in a series of mouse brains extracted at different times (15, 30, 60, and 120 min). This is presumably because of stimulation of phospholipase enzymes under ischemic conditions [64,65].

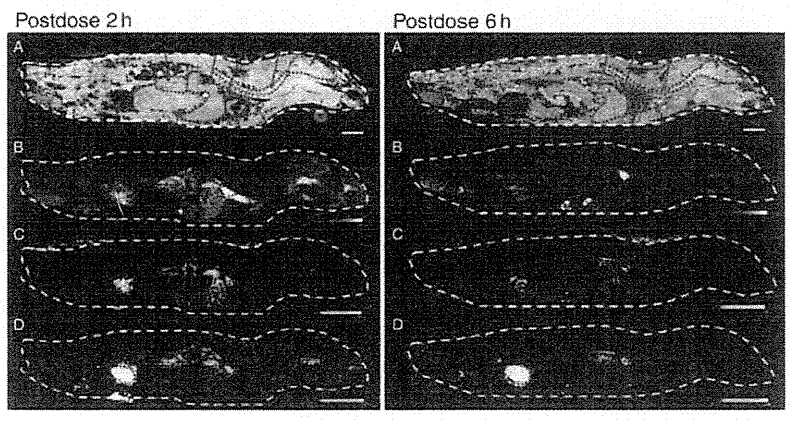

FIGURE 3.25 Detection of the drug olanzapine and its metabolite distribution in a whole-body sagittal tissue section by single IMS analysis [2]. A. Optical images of tissue sections from rats 2 and 6 h after treatment with olanzapine, across four gold MALDI target plates. Organs are outlined by dashed lines, and a dot is used as a time point label. B. MS/MS ion image of olanzapine (*m/z* 256). C. MS/MS ion image of N-desmethyl metabolite (*m/z* 256). D. MS/MS ion image of 2-hydroxymethyl metabolite (*m/z* 272). Bar denotes 1 cm.

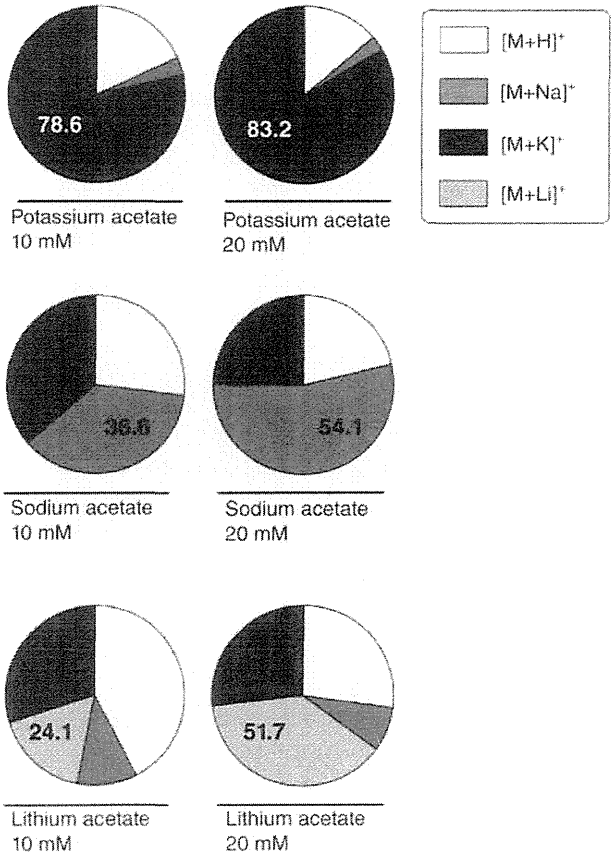

FIGURE 3.26 Potassium forms a stronger adduct with PC molecules than did sodium and lithium. To determine optimum experimental condition of using alkali metal salt as matrix additive, we added potassium, sodium, and lithium salts in various concentrations to the matrix solution. We then sprayed matrix solutions containing potassium, sodium, and lithium acetate in various concentrations (10 and 20 mM) on the tissue sections. The circular charts present the proportion of ion intensities of $[M+H]^+$, $[M+Na]^+$, $[M+K]^+$, and $[M+Na]^+$ ion of lyso-PC(17:0), which was dispensed on the brain homogenate slice ($n = 3$). Potassium dominantly formed an adduct with the PC molecule upon addition of 10 mM potassium acetate; on the other hand, other types of PC ions still accounted for approximately half upon the addition of 20 mM sodium and lithium acetate.

3.3.2.2 Preparation of Tissue Sections The process of preparing sections for IMS measurement is essentially similar to that used in the preparation of frozen sections for immunostaining or dye staining. However, since the sections created in this case are served to MS measurement, there are certain essential differences compared to the section-preparation techniques used in other staining methods, as summarized in Table 3.5.

A point to bear in mind is that IMS is an imaging technique based on MS, a microchemical analytical technique.

1. Usually, tissue blocks are held by an optimum cutting temperature (OCT) polymer, but tissues should not be embedded into such polymer reagent because any residual polymer on the tissue slices degrade the mass spectra for both protein and small molecular analysis [10] (see Note 1).
2. Wipe off any oil remaining on the blade with ethanol and carefully attach the blade to the cryostat (here we used CM 3050; Leica, Wetzler, Germany).
3. Precool the forceps and brushes by placing them inside the cryostat.
4. Adjust the several conditions of cryostat and try sectioning. (e.g., the position of the antiroll and blade, angle of the sample, and chamber temperature, etc). If sections tend to curl up, the temperature is too high or the antiroll is placed inappropriately (Figure 3.28).
5. In this study, tissues blocks were sectioned at −16°C to a thickness of 5 μm [10,66].
6. Try cutting and determine the optimal tissue thickness (see Note 2).
7. Keep the slice under the antiroll for a while, until it no longer curls.
8. Put the ITO-coated glass slides (Bruker Daltonics) into the chamber, immediately place the slides over the tissue slice, and paste tissues on it (Figure 3.28).
9. Keep performing thin-sectioning and pasting.
10. Bring out the slides with tissues, and immediately dry them in a stream of nitrogen gas. Insufficient drying causes the sample to peel off.
11. Serve the slice to the next process (washing process for protein analysis or matrix application for small molecule analysis).

Notes:

1. Embedding enables the sample to retain its shape and makes the cutting process easier. However, in IMS experiments, attachment and penetration of the embedding agents (e.g., OCTs) in the samples can lead to a deterioration of the MS signals [4,10] (Figure 3.29A). In particular, when analyzing small molecules with an m/z 800–2000, contamination with OCT highly abundant signals that correspond to the polymer in the positive ion

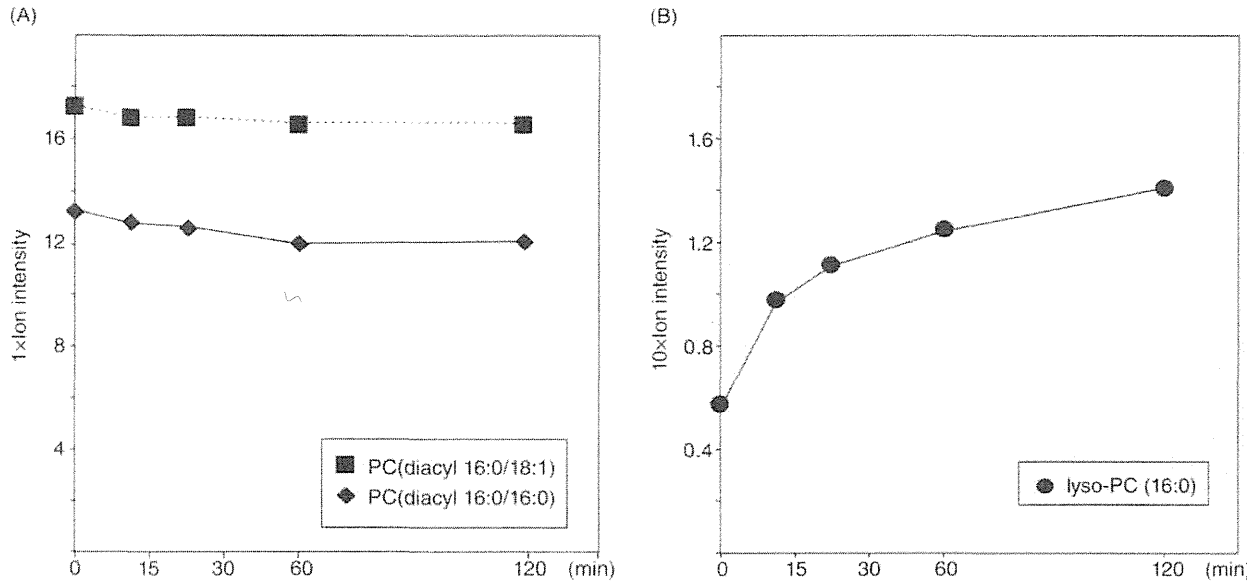

FIGURE 3.27 Postmortem degradation of GPLs observed by IMS. GPLs were degraded within 15 min in a series of mouse brains extracted at different times (15, 30, 60, and 120 min) (A). Conversely, lyso-PC was increased during the period (B) [64,65].

TABLE 3.5 The Major Cautionary Points at Each Step of Slice Preparation

Procedure for Preparing a Frozen Section for IMS
Tissue extraction
Because of rapid metabolic turnover, tissues should be handled in a fixed time course, particularly for the analysis of small molecules.
↓
Embedding
Avoid the use of polymeric compounds, such as optimum cutting temperature (OCT) compound, for embedding [4,10]. As an alternative, a precooled semiliquid gel of 2% sodium carboxymethylcellulose (CMC) can be used as an embedding compound, as it does not interfere with MS [63].
↓
Sectioning
Tissue thickness < 20 μm improves spectrum quality [66].
↓
Mounting
The use of conductive materials is recommended for supporting the tissue section [91][a].
↓
Washing
By removing small molecules such as lipids, the tissue-washing process improves the spectrum quality for protein/peptide detection [9–11].
↓
Drying
Failure to dry sections sufficiently may cause samples to peel off in the vacuum chamber of the mass spectrometer.
↓
Sputtering
Sputtering of metals (e.g., gold) onto tissue sections before/after the matrix application process improves the spectrum quality [63,72].

[a] Some instruments support the use of nonconductive materials [1].

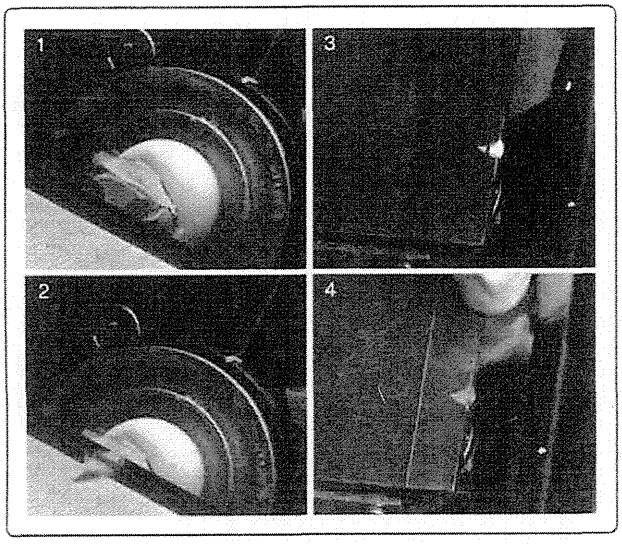

FIGURE 3.28 Cutting thin sections with cryostat. 1. Cutting tissues into optimal tissue thickness. 2. Keep the slice under the antiroll for a while, until it no longer curls. 3 and 4.Put the indium tin oxide (ITO)-coated glass slides into the chamber, immediately place the slides over the tissue slice, and paste tissues on it.

mass spectra would virtually mask the analyte signal. This virtually hides all of the smaller peaks (Figure 3.29B). For this reason, when preparing sections for IMS, OCT is used only to "support" the tissue blocks and, thus, OCT does not directly attach to the tissue being analyzed. As an alternative, a precooled semiliquid gel of 2% sodium CMC can be used as an embedding compound that does not interfere with MS [63].

2. Slice thickness is the most important factor associated with IMS measurement. When the thickness of a slice is >15 μm, the sensitivity deteriorates, particularly when high molecular weight proteins are analyzed [66] (Figure 3.30). This difference can be attributed to a phenomenon referred to as the "charging effect" [67]. Generally, biological tissue sections have low intrinsic electric conductivity, and this tendency is considered more apparent with thicker tissue sections. In this state, a surplus electric charge generated by laser irradiation is not lost through the sample stage. Thus, multiple charged ions are generated—and ultimately leads to a significant loss of sample ions that would otherwise reach the detector [67]. However, a high technical proficiency is required in order to prepare slices with thicknesses of several micrometers each. Currently, most samples are prepared with a slice thickness of 10–20 μm [68,69]. These medium-thick sections appear to provide a good compromise between optimal IMS performance and experimental efficiency [70], particularly when a large number of samples need to be analyzed [71]. The "metal sputtering" technique enhances the signal intensity and thus image quality [63,72], presumably by avoiding the "charging effect."
3. Dehydration of tissue sections for long times can lead to altered signals [73]. Goodwin and colleagues demonstrated that, even within 1 min, signals were altered, both increasing and decreasing. Therefore, tissue slices should be moved to the next step (matrix application) as quickly as possible. Considerable care is required at these stages in order to facilitate a comparison between the biomarkers in independent IMS experiments.

3.3.2.3 Spray-Coating of the Matrix Solution with an Artistic Airbrush Among the several matrix application methods, the spray-coating method is one of the frequently used methods. In this process, an entire tissue section can be coated with relatively small crystals homogenously. For this operation, several instruments, including TLC sprayers and artistic airbrushes, are available.

To achieve optimal spraying: (1) minimize the droplet size, to accelerate the dry rate, (2) keep the airbrush in a position at same distance from tissue, and (3) gradually move the airbrush horizontally. Further technical tip to bear in mind when executing this method is to maintain equilibrium between the two rates—one rate, at which a fine aerosol of airbrushed matrix solution slightly moisturizes the tissue section which facilitates analyte extraction, and the other rate, at which the quick solvent evaporates which prevent analyte migration (Figure 3.31 inset). To execute this, important parameters to care for practical spraying include (1) the size of the droplet, (2) the amount of the mist, (3) the angles and distances between the spray nozzle and the tissue section, and (4) laboratory temperature and humidity. These parameters are described below in detail.

Preparation of Matrix Solution

1. Weigh appropriate amount of matrix compound and put it into an organic solvent-tolerant microtube.
2. Add 1.0 mL of solvent with organic solvent-tolerant pipette tips.
3. Dissolve the matrix compound thoroughly by vortexing or performing brief sonication.
4. Store at room temperature until use.

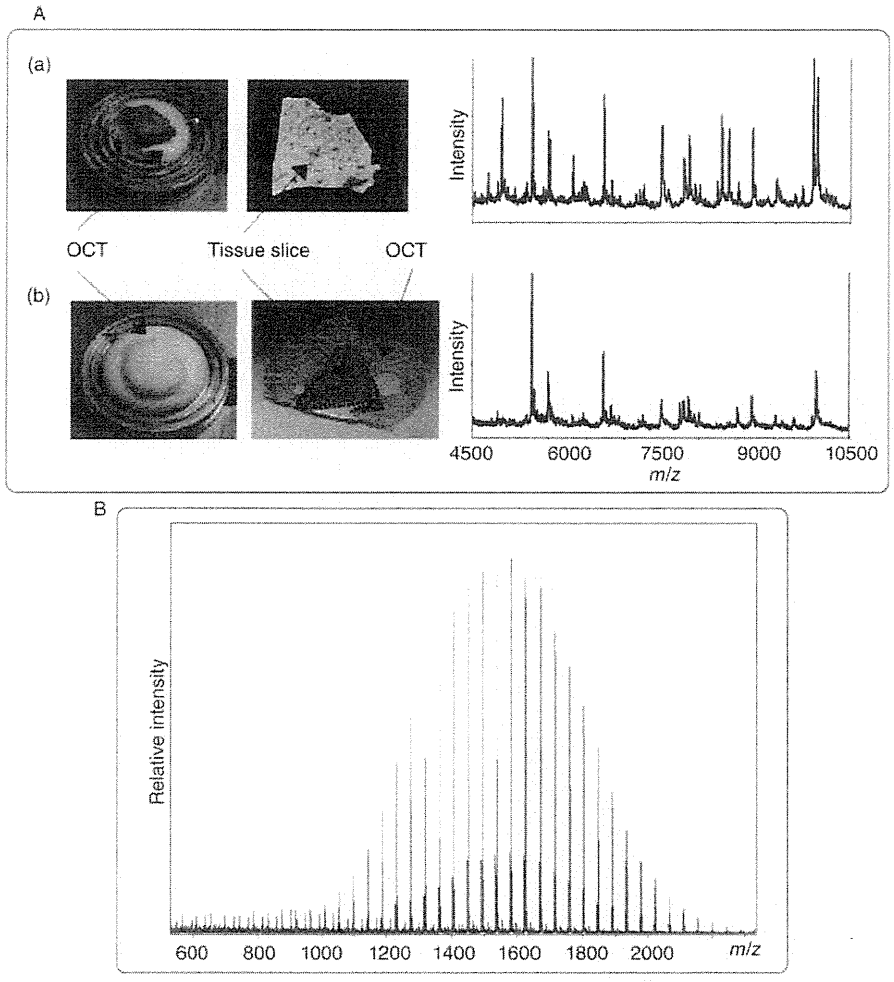

FIGURE 3.29 Residual OCT polymer on the tissue slices degrades the mass spectra. A. Decrease in detection sensitivity of the ions originating from proteins due to contamination with OCT. OCT adhering to the tissue section diminishes the detectable peaks. (a) A case in which OCT was used only for supporting the tissue block. (b) A case in which the tissue block was completely embedded with OCT. B. Contamination with OCT leads to the presence of extremely high polymer peaks.

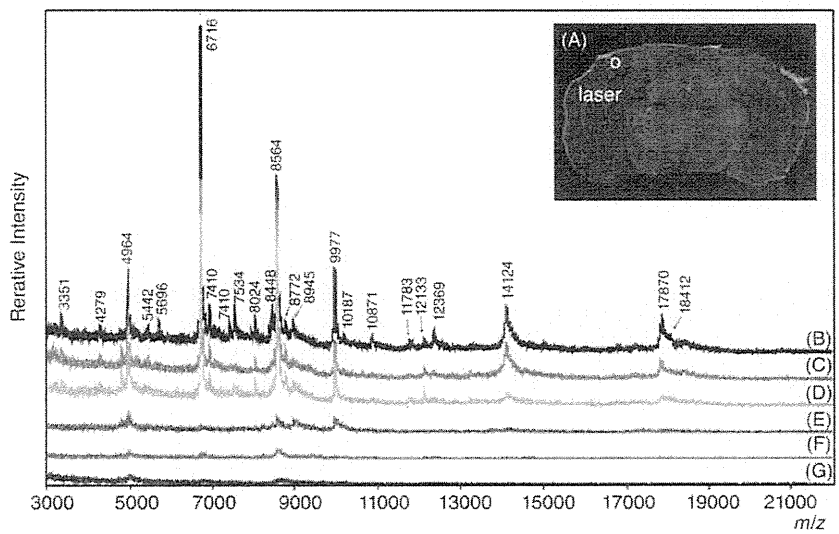

FIGURE 3.30 Mass spectra obtained from the cerebral cortex region [66]. The mass spectra obtained from the cerebral cortex region in mouse brain slices (a white circle in (A) with thicknesses of 2 μm (B), 5 μm (C), 10 μm (D), 15 μm (E), 30 μm (F), and 40 μm (G). A larger number of mass peaks with high signal-to-noise (S/N) ratios were observed in the spectra obtained from sections with 2, 5, and 10 μm thicknesses than in those obtained from sections with 15, 30 and 40 μm thicknesses.

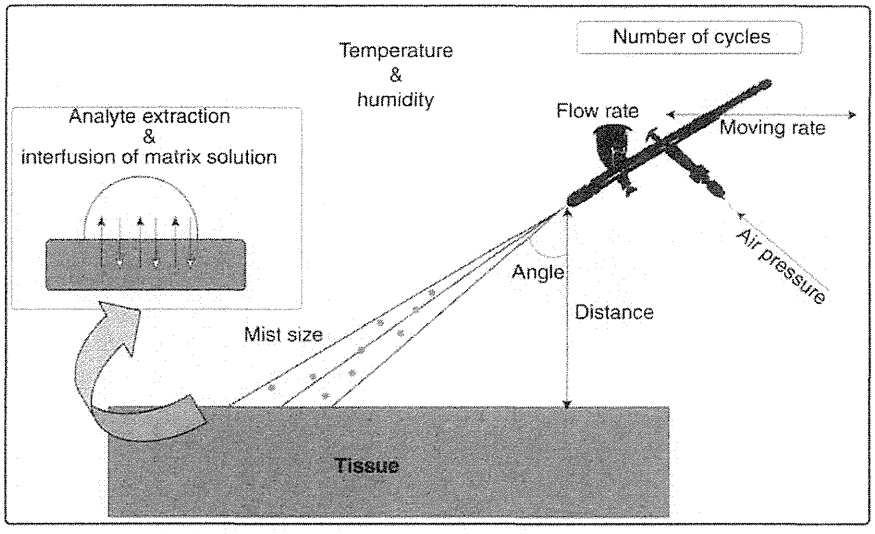

FIGURE 3.31 Representative parameters of spraying operation with an airbrush, required to be controlled among the trials for the reproducible IMS experiment.

Notes:

- Microtubes with organic solvent-tolerant properties can be purchased from Eppendorf Co., Ltd.
- Use HPLC or LC/MS-grade solvent for preparing matrix solution.
- Preparing the matrix solution on the day of experiment is recommended.

Matrix Application Using an Airbrush

1. Pour approximately 1.0 mL of the solvent for the matrix solution into the airbrush.
2. Optimize the size of the droplet, the amount of mist, and the angles and distances between the nozzle and the sample.
3. Remove the solvent from the airbrush.
4. Mask the areas outside of the tissue section, which is mounted on the ITO slide glass, with a masking tape.
5. Fix the masked ITO slide glass onto a perpendicular board.
6. Pour the prepared matrix solution into the airbrush and spray onto the tissue section on the ITO slide glass.
7. As a rough guide for optimal coating, spray approximately 0.5–1.0 mL of matrix solution for one ITO slide glass.
8. Remove the masking tape from the ITO slide glass after spraying, and place the sample in an airtight container with dry silica gel.
9. Perform the IMS measurement as soon as possible to minimize the progress of sample damage.
10. Figure 3.32 shows an example of good and unfavorable spraying results by spraying DHB matrix solution (50 mg/mL, 70% MeOH containing 10 mM potassium acetate).

3.3.2.4 Spectrum Normalization In the data analysis of MALDI-IMS, experimenters should not interpret peak intensities of each metabolite simply as metabolite concentrations. Dr. R. Murphy explained this issue using a following equation. Observed ion intensities were result of not only metabolite concentration, but also functions of ionization efficiency of each metabolite compound and local environmental factors [74]:

$$\text{Intensity}_{m/z} = f([\text{metabolite conc.}]\times[\text{ionization cross-section}]\times[\text{local environment}]\times\ldots).$$

In this equation, local environmental factors include analyte extraction efficiency from the distinct tissue structures, and as the most important factor, the matrix crystal condition. Figure 3.33 shows scanning electron microscope (SEM) images of DHB crystals on the tissue section as a result of manual spraying of the matrix solution. Although the presented manual spraying result could be classified into "good" example (like that shown in Figure 3.31A), as can been seen, the SEM observation revealed rather heterogeneous distribution of DHB crystals on the tissue surface. If tissue surface is scanned with a typical MALDI laser, there could be "hot spot" in which more ions were detected than other location,